Journal of Advanced Research 65 (2024) 153–165

Contents lists available at ScienceDirect

Journal of Advanced Research

journal homepage: www.elsevier.com/locate/jare

Loss of *Sc5d* results in micrognathia due to a failure in osteoblast differentiation

Chihiro Iwaya [a,b,1], Akiko Suzuki [a,b,1,2], Junichi Iwata [a,b,c,*]

[a] Department of Diagnostic & Biomedical Sciences, The University of Texas Health Science Center at Houston, School of Dentistry, Houston, TX 77054, USA
[b] Center for Craniofacial Research, The University of Texas Health Science Center at Houston, School of Dentistry, Houston, TX 77054, USA
[c] MD Anderson Cancer Center UTHealth Graduate School of Biomedical Sciences, Houston, TX 77030, USA

HIGHLIGHTS

- *Sc5d*$^{-/-}$ mice exhibit mandibular hypoplasia resulting from defects in osteoblast differentiation.
- Cholesterol metabolism plays a crucial role in bone development through the formation of primary cilium, a cell surface structure that senses extracellular cues.
- The activation of hedgehog and WNT/β-catenin signaling pathways, which induce expression of osteogenic genes *Col1a1* and *Spp1*, is compromised in the mandible of *Sc5d*$^{-/-}$ mice.
- Treatments with an inducer for hedgehog or WNT/β-catenin signaling or simvastatin, a drug that restores abnormal cholesterol productions, partially rescue the defects in osteoblast differentiation seen in *Sc5d*$^{-/-}$ cells.

GRAPHICAL ABSTRACT

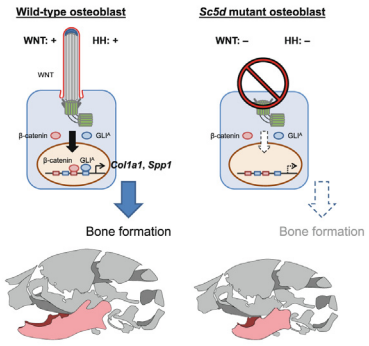

ARTICLE INFO

Article history:
Received 6 September 2023
Revised 30 November 2023
Accepted 9 December 2023
Available online 10 December 2023

Keywords:
Craniofacial bone formation
Cholesterol metabolism
Sc5d
Mandible hypoplasia
Primary cilia

ABSTRACT

Introduction: Mutations in genes related to cholesterol metabolism, or maternal diet and health status, affect craniofacial bone formation. However, the precise role of intracellular cholesterol metabolism in craniofacial bone development remains unclear.
Objective: The aim of this study is to determine how cholesterol metabolism aberrations affect craniofacial bone development.
Methods: Mice with a deficiency in *Sc5d*, which encodes an enzyme involved in cholesterol synthesis, were analyzed with histology, micro computed tomography (microCT), and cellular and molecular biological methods.
Results: *Sc5d* null mice exhibited mandible hypoplasia resulting from defects in osteoblast differentiation. The activation of the hedgehog and WNT/β-catenin signaling pathways, which induce expression of osteogenic genes *Col1a1* and *Spp1*, was compromised in the mandible of *Sc5d* null mice due to a failure in the formation of the primary cilium, a cell surface structure that senses extracellular cues. Treatments

* Corresponding author at: 1941 East Road, BBS 4208, Houston, Texas 77054, USA.
E-mail address: Junichi.Iwata@uth.tmc.edu (J. Iwata).
[1] These authors equally contributed to this study.
[2] Current affliation: University of Missouri-Kansas City, School of Dentistry, Kansas City, Missouri 64108, USA.

https://doi.org/10.1016/j.jare.2023.12.008

with an inducer of hedgehog or WNT/β-catenin signaling or with simvastatin, a drug that restores abnormal cholesterol production, partially rescued the defects in osteoblast differentiation seen in *Sc5d* mutant cells.

Conclusion: Our results indicate that loss of *Sc5d* results in mandibular hypoplasia through defective primary cilia-mediated hedgehog and WNT/β-catenin signaling pathways.

Introduction

Cholesterol, which is abundant in cellular membranes, is responsible for their properties and plays a role in membrane trafficking. More than 20 enzymatic reactions are involved in cholesterol biosynthesis and degradation through negative and positive feedback mechanisms [1]. Mutations in the human lathosterol 5-desaturase (SC5D) gene, which catalyzes the conversion of lathosterol to 7-dehydrocholesterol in the second to last step of endogenous cholesterol synthesis, cause lathosterolosis, a disease characterized by craniofacial abnormalities, microcephaly, cataracts, and skeletal defects [1]. Although the metabolites and enzymes in cholesterol metabolic pathways play a crucial role in osteogenesis [2], it remains unclear how cholesterol metabolism aberrations contribute to craniofacial bone formation. Interestingly, *Sc5d*$^{-/-}$ mice die at birth with various malformations, including cleft palate, micrognathia, and abnormal limb formation [3].

The bone extracellular matrix contains collagens, which provide a specific niche for the resident cells to function, and their production is regulated through a series of multiple regulatory pathways [4]. The primary cilium, a cholesterol-enriched antenna-like structure that senses extracellular cues on cell surfaces, recruits and retains receptors and membrane proteins [5] and serves as a signaling center for various signaling pathways, including hedgehog (HH) and WNT/β-catenin signaling. Defects in primary cilia lead to a group of disorders associated with ciliary abnormalities (a.k.a. ciliopathies) characterized by craniofacial anomalies such as micrognathia, craniosynostosis, hypertelorism, and cleft palate, as well as immature lungs and enlarged bladders [6,7]. The primary cilium comprises the axoneme, motor dynein and kinesin, cargos, and the ciliary membrane, which is a cholesterol-enriched membrane distinct from the plasma membrane. Phenotypic similarities between ciliopathies and *Sc5d* deficiency in mice suggest that cholesterol metabolism plays a crucial role in bone development through the primary cilium. In this study, we show that cholesterol metabolism aberrations inhibit osteogenesis due to a failure in HH and WNT/β-catenin signaling associated with the primary cilia in *Sc5d* null mice.

Materials and methods

Animals

The *Sc5d*$^{-/-}$ mice were a gift from Dr. Forbes D. Porter (The Eunice Kennedy Shriver National Institute of Child Health and Human Development, National Institutes of Health, Bethesda, Maryland, USA). *Gli1-LacZ* (JAX, 008211) and *Topgal* (JAX, 004623) reporter mice were purchased from The Jackson laboratory. Genotyping was performed by PCR, as previously described [3]. *Sc5d*$^{+/-}$ females were placed with adult *Sc5d*$^{+/-}$ males with proven fertility overnight and examined the following morning for vaginal plugs as E0.5. We analyzed embryos at E12.5, E13.5, E14.5, and E18.5 stages independently. n = 6 per group from different litters in each experiment. All mice were bred under pathogen-free conditions, with free access to water and food and a 12 h light/12 h dark cycle. Carbon dioxide (CO_2) inhalation was used as the method for euthanasia. All mice were maintained in the animal facility of UTHealth.

Ethics statement

All animal experiments were reviewed and approved by the Animal Welfare Committee (AWC) and the Institutional Animal Care and Use Committee of UTHealth (AWC 22–0087).

microCT scanning and three-dimensional (3D) reconstruction

Fixed E18.5 mouse embryos were placed in a 12-mm diameter sample holder and stabilized with polypropylene straws during the scan (n = 6 per group). microCT scan was performed at a 12 μm resolution using a SCANCO microCT-40 system (SCANCO Medical USA Inc., USA; 55 kVp and 145-μA). 70 % ethanol was used as scan medium. 3D reconstruction and analysis of the microCT images were performed using the Dragonfly software [Version 2021.1 for Windows, Object Research Systems (ORS) Inc., Montreal, Canada] with DICOM files. The landmarks used in length and height measurements of the mandible were: 1. most anterior point of the mandible; 2. molar alveolus of dentary; 3. inferior point of the mandibular body; and 4. posterior point of the condylar process. Mandible length was determined from the distance between landmarks 1 and 4; mandible height was determined from the distance between landmarks 2 and 3.

Skeletal staining

The 3D architecture of the skeleton was examined by modified whole-mount Alcian blue-Alizarin Red S staining of E18.5 mouse embryos, as previously described [8].

Histology

Mouse embryos (E12.5 to E18.5) were fixed in 4 % paraformaldehyde, decalcified with 10 % ethylenediaminetetraacetic acid disodium dihydrate, embedded in paraffin and sectioned at 4 μm thickness. Hematoxylin and Eosin staining and immunohistochemistry were performed as previously described [8]. The list of antibodies used in this study is included in Table S1. Apoptotic cells were detected using terminal deoxynucleotidyl transferase dUTP nick end labeling (TUNEL) staining (Click-iT Plus TUNEL Assay with Alexa 594; C10618, molecular probes), performed according to the manufacturer's protocol. A total of six fields, which were randomly selected from three independent experiments, was used for the quantification of BrdU, Ki-67, and TUNEL-positive cells. Beta-galactose staining was performed in E13.5 *Sc5d*$^{-/-}$*;Gli1-LacZ*, *Sc5d*$^{+/+}$*;Gli1-LacZ*, *Sc5d*$^{-/-}$*;Topgal*, and *Sc5d*$^{+/+}$*;Topgal* mice, as previously described [8]. Fluorescence images were captured with a confocal microscope (Ti-C2, Nikon), and color images with a light microscope (BX43, Olympus).

Immunoblotting

The mandibles were microdissected from WT and *Sc5d*$^{-/-}$ mice at E14.5 and E18.5, and proteins were extracted with RIPA buffer (Thermo Fisher Scientific) containing a protease inhibitor cocktail (04693159001, Roche) and centrifuged at 800 × *g* for 3 min at 4 °C. The protein concentration of the supernatants was measured with the BCA protein kit (Thermo Fisher Scientific). Protein samples (20 μg) were applied to Mini-PROTEAN TGX Gels (Bio-Rad Laboratories) and transferred to a polyvinylidene difluoride membrane. All immunoblotting experiments were performed three times to validate the results. The list of antibodies used in this study is included in Table S1.

Quantitative RT-PCR

Total RNAs isolated from the mandible, which was microdissected from WT and *Sc5d*$^{-/-}$ mice at E12.5, E13.5 and E14.5, or from primary osteoblasts cultured in osteogenic differentiation medium for 7 days, were extracted with the QIAshredder and RNeasy mini extraction kit (QIAGEN), as previously described [9]. Housekeeping gene *Gapdh* was used as an internal control. The ΔΔ-CT method was applied for the analyses. The list of the RT-PCR primers used in this study is included in Table S2.

In situ hybridization

Embryos were fixed with 4 % paraformaldehyde, embedded in paraffin, and sectioned at 4 μm thickness. *In situ* hybridization analyses were performed using probes for *Gli1* (ACD, 311001-C3), *Ptch1* (ACD, 402811), *Lef1* (ACD, 441861), and *Axin2* (ACD, 400331) using the RNAscope 2.5 Assay platform (ACD). The color images were captured with a light microscope (BX43, Olympus).

Comparative analysis of transcription factor binding sites

The UCSC genome browser (https://genome.ucsc.edu/) was used to obtain the genomic sequences of the murine genes (Build 38), including the 10 kb sequence upstream of the respective transcription start site. The sequence was then mapped to human (Build 38) and rat (Build 6.0) genomes with the BLAST tool, as previously described [8]. The multiple alignments were obtained using the Clustal Omega tool with default parameters and settings. LEF1-binding motifs (minimal core sites: 5′-CAAAG-3′ and 5′-CTTTG-3′; optimal sites: 5′-CTTTGWW-3′ and 5′-WWCAAAG-3′, W = A/T) and the GLI-binding motif (5′-CACCACCCA-3′) were searched in the aligned DNA sequences, as previously described [8–11].

ChIP assay

At Day 3 of osteogenic differentiation, osteoblast extracts were incubated with either LEF1/active β-catenin (8814, Cell Signaling Technology), GLI1 (ab49314, Abcam), or normal rabbit IgG (2729, Cell Signaling Technology) as a negative control. The ChIP assay was performed as previously described [8]. The putative LEF1/β-catenin or GLI binding sites in the immune complexes were detected by PCR using specific primers. Antibody and primer information is provided in Table S1 and S2. The positions of the PCR fragments correspond to NCBI mouse genome Build 38 (mm 10).

Cell culture

Primary osteoblasts were obtained from calvaria from newborns and maintained in minimum essential medium α (MEM-α; Sigma Aldrich) supplemented with 10 % fetal bovine serum (FBS), penicillin/streptomycin (A5955, Sigma Aldrich), and L-glutamine (35050061, Gibco) at 37 °C in a humidified atmosphere with 5 % CO_2, as previously described [8]. For osteogenic differentiation, osteoblasts were cultured in 12-well plates or 3-cm dishes, and osteogenic differentiation was induced with osteogenic induction medium, i.e. MEM-α supplemented with 100 μg/mL L-ascorbic acid (A4544, Sigma Aldrich), 5 mM beta-glycerophosphate disodium salt hydrate (G9422, Sigma Aldrich), 10 % cholesterol-free FBS, penicillin/streptomycin, and L-glutamine for 14 and 28 days. To evaluate osteogenic differentiation, alkaline phosphatase, Alizarin Red, and von Kossa staining was performed at 14 and 28 days, as previously described [8]. To evaluate WNT and HH signaling activity, osteoblasts were cultured without serum for 24 h and then treated with either 20 mM lithium chloride (LiCl), 5 nM Smoothened agonist (SAG, 566660, Sigma Aldrich), or 20 mM NaCl (a negative control) in serum-free medium for 24 h. WNT3A treatment was performed as previously described (8). Regarding the rescue experiments, osteoblasts were starved of serum for 24 h and then treated with 30 mM simvastatin (567022, Calbiochem-Sigma Aldrich), followed by immunofluorescence staining, quantitative RT-PCR, immunoblotting, and osteogenic differentiation assays with Alizarin Red staining. To induce ciliogenesis, osteoblasts were starved of serum for 24 h, followed by immunofluorescence staining or collection of total RNA and protein. For the cell proliferation assay, osteoblasts were plated onto 96-well plates at a density of 5,000 cells per well and then counted by CCK8 (Dojindo Molecular Technologies) at 24, 48, and 72 h.

Statistical analysis

All results were obtained from at least three independent experiments (n = 6 per group in each experiment). All experimental data were analyzed with the Prism software (GraphPad Software, California, USA). The statistical significance of the differences between two groups (control and treated groups) was evaluated using a two-tailed Student *t* test adjusted by Tukey's test. The statistical significance for multiple pairs of groups was evaluated using a one-way analysis of variance (ANOVA) with Tukey's test. An adjusted $p < 0.05$ was considered to be statistically significant. Data are represented as mean ± standard deviation in the graphs.

Results

Micrognathia in Sc5d null mice

Sc5d knockout (KO) mice exhibited craniofacial deformities, including cleft palate, open eyelids, short head, and micrognathia (extremely short bone in the anterior half of mandible) (Fig. 1A). In addition, *Sc5d* KO mice exhibited limb abnormalities (either syndactyly or polysyndactyly) in both forelimbs and hindlimbs, as well as defects in endochondral ossification in the radius/ulna and tibia/fibula (Fig. S1). To investigate bone formation in *Sc5d* KO mice, we performed skeletal staining and found that craniofacial bones, especially the mandible, in E18.5 *Sc5d* KO mice were smaller than the ones in wild-type (WT) control mice, with less mineralized frontal and parietal bones and no calcification in the intraparietal bone (Fig. 1B). The size and shape of the mandible were further evaluated with reconstructed 3D micro-computed tomography (microCT) analyses in *Sc5d* KO and WT control mice. We found that the mandible in *Sc5d* KO mice was shorter in length [distance between the most anterior point of the mandible (#1) and the posterior point of the condylar process (#4)], accompanied by the volume and surface area of the mandible, although the height [distance between the molar alveolus of dentary (#2) and the infe-

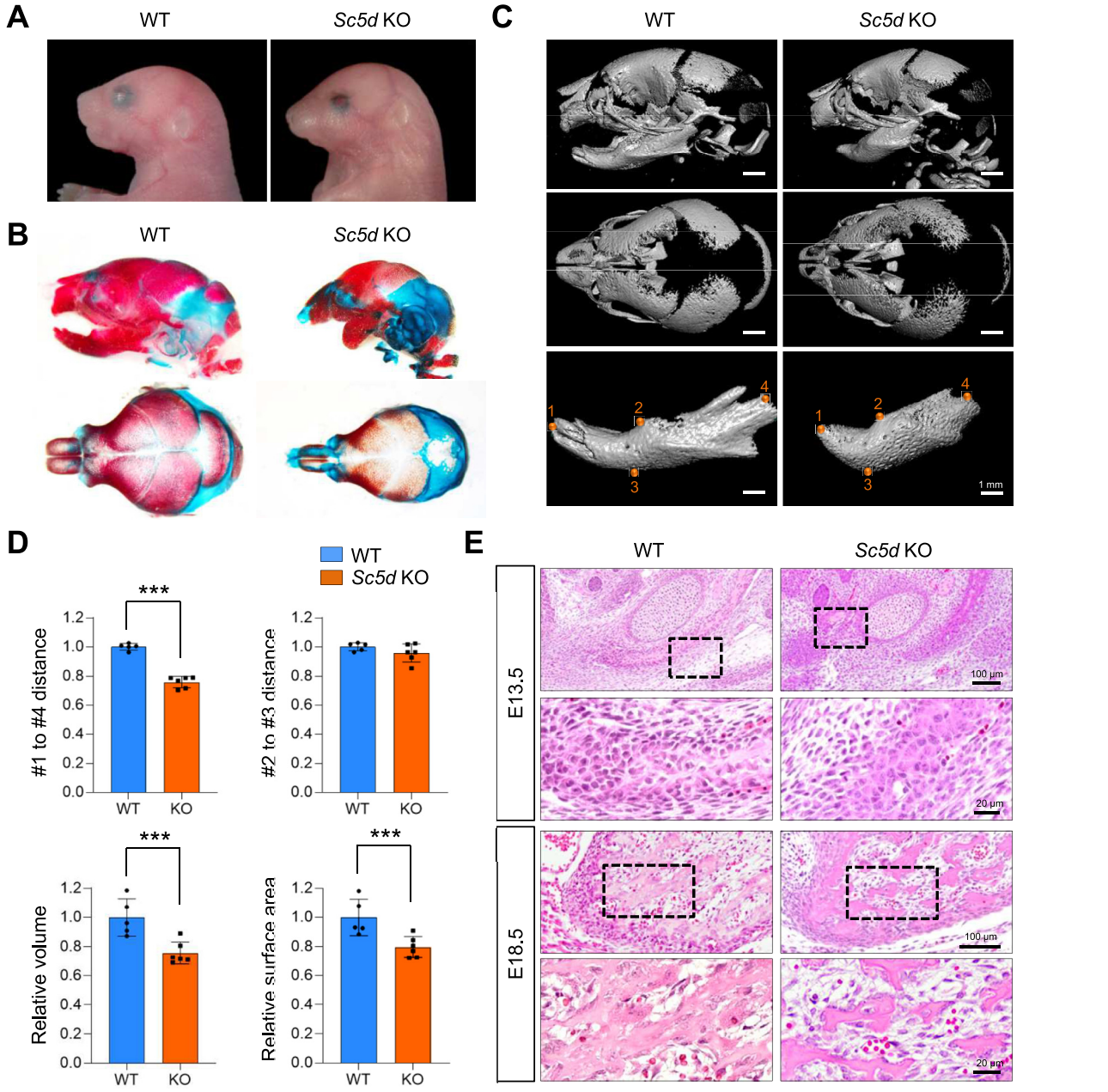

Fig. 1. Osteogenesis defects in *Sc5d* null mice. (*A*) Side view of the craniofacial region of E18.5 *Sc5d* null (right) and wild-type (WT) control (left) mice. (*B*) Skeletal staining with Alcian blue (cartilage) and Alizarin red S (bone) in E18.5 *Sc5d* null (right) and WT control (left) mice. Side view (top panels) and top view of the calvaria (bottom panels). (*C*) MicroCT images of the skull in E18.5 *Sc5d* null (right) and WT control (left) embryos. Side view (top panels), top view of the calvaria (middle panels), and mandible (bottom panels); Scale Bar: 1 mm 1. Most anterior point of the mandible; 2. molar alveolus of dentary; 3. inferior point of the mandibular body; 4. posterior point of the condylar process. (*D*) Measurement of height (2 – 3) and length (1 – 4) of the mandible in (*C*). WT (blue bars) and *Sc5d* null (orange bars). ***$p < 0.001$. (*E*) Hematoxylin and Eosin staining in *Sc5d* null (right) and WT control (left) mice at E13.5 and E18.5. The boxed areas are enlarged. Scale bars, 100 μm in top panels and 20 μm in bottom panels. (For interpretation of the references to color in this figure legend, the reader is referred to the web version of this article.)

rior point of the mandibular body (#3)] was not significantly altered in *Sc5d* KO mice compared with WT (Fig. 1C, D). Histological analyses showed that although osteoblast condensation at the osteogenic front occurred normally in the mandible of *Sc5d* KO mice, intramembranous ossification around the Meckel's cartilage was compromised in *Sc5d* KO mice, resulting in a reduced calcified bone area in E18.5 *Sc5d* KO mice compared to WT control mice (Fig. 1E).

Unaltered cell survival in Sc5d KO mice

There are several possible causes for the micrognathia phenotype in *Sc5d* KO mice: reduced cell proliferation, increased cell death, dysregulated osteoblastogenesis, or a combination of these. To determine the cellular mechanism underlying the bone defects in *Sc5d* KO mice, we performed BrdU incorporation assays in *Sc5d* KO and WT control mice at E12.5, E13.5, and E14.5 and found that there was no defect in cell proliferation at the active site of intramembranous ossification of the mandible in *Sc5d* KO mice (Fig. 2A, B). We further confirmed that there were no cell proliferation defects in our immunohistochemical analysis for Ki67 in *Sc5d* KO osteoblasts labeled with RUNX2, an early osteoblast marker (Fig. S2A, B). Furthermore, cell proliferation defects in *Sc5d* KO osteoblasts were confirmed by cell proliferation assays using primary osteoblasts isolated from the calvaria of *Sc5d* KO and WT control mice (Fig. S3A). In addition, there was no change in cell death

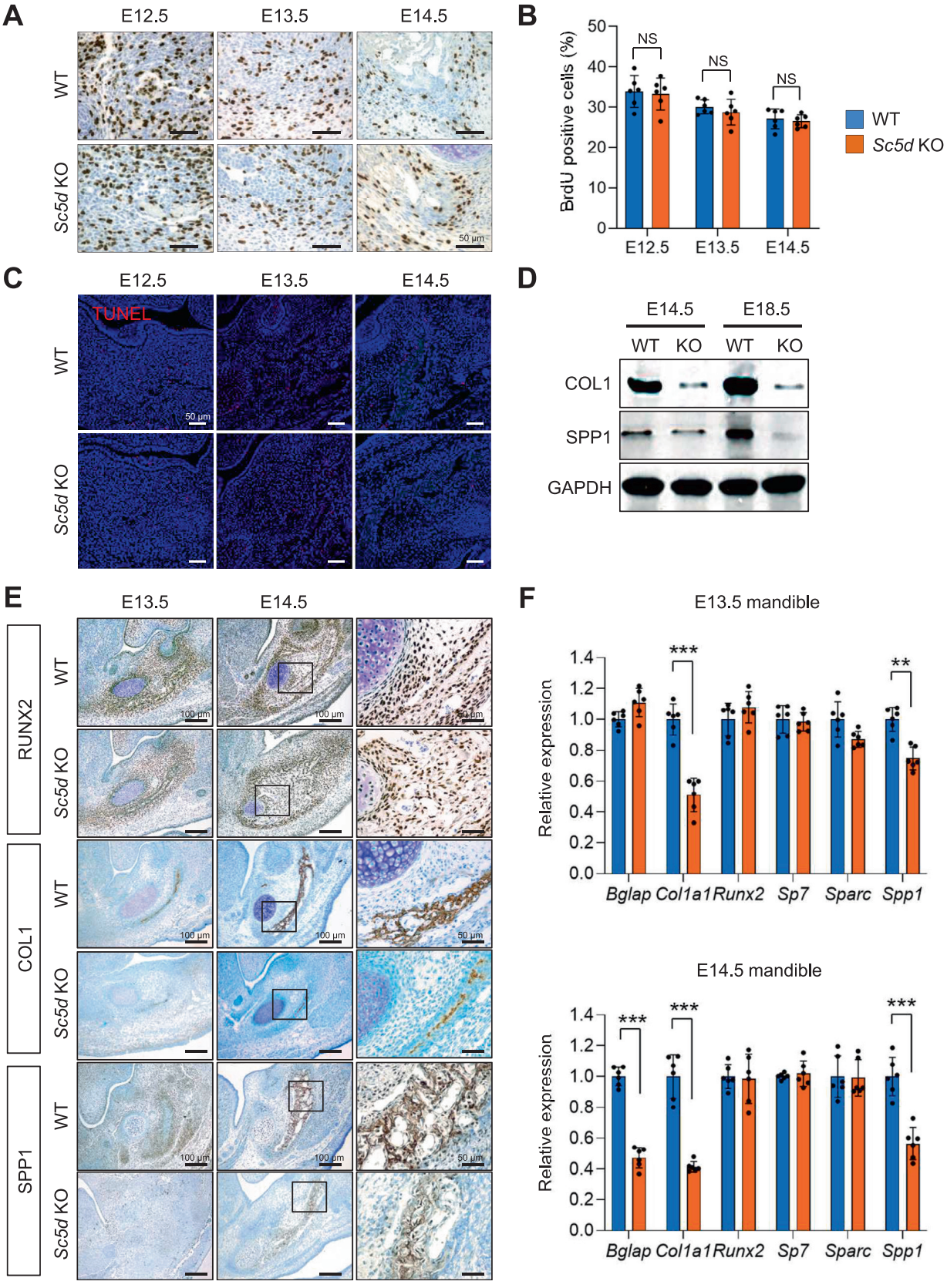

Fig. 2. Suppression of osteoblast differentiation and collagen expression in *Sc5d* null mice. (*A*) BrdU incorporation assays at the intramembranous ossification region of the mandible in *Sc5d* null (bottom) and WT control (top) mice at E12.5, E13.5, and E14.5. Methylene blue was used for counterstaining. Scale bars, 50 μm. (*B*) Quantification of BrdU-positive cells per total number of cells (%) in *B*. WT (blue bars) and *Sc5d* null (orange bars). NS: not significant. (*C*) TUNEL staining (red) at the intramembranous ossification region of the mandible in *Sc5d* null (bottom) and WT control (top) mice at E12.5, E13.5, and E14.5. Scale bars, 50 μm. (*D*) Immunoblotting of COL1, SPP1, and GAPDH (internal control) in the mandible of *Sc5d* null (KO) and WT control mice at E14.5 and E18.5. (*E*) Immunohistochemical staining for RUNX2, COL1, and SPP1 at the intramembranous ossification region of the mandible in *Sc5d* null and WT control mice at E13.5 and E14.5. Methylene blue was used for counterstaining. Scale bars, 100 μm. (*F*) Relative mRNA expression of the indicated osteoblast differentiation markers in the mandible of *Sc5d* null (orange bars) and WT control mice (blue bars) at E13.5 and E14.5. $^{***}p < 0.001$. n = 6 per group. (For interpretation of the references to color in this figure legend, the reader is referred to the web version of this article.)

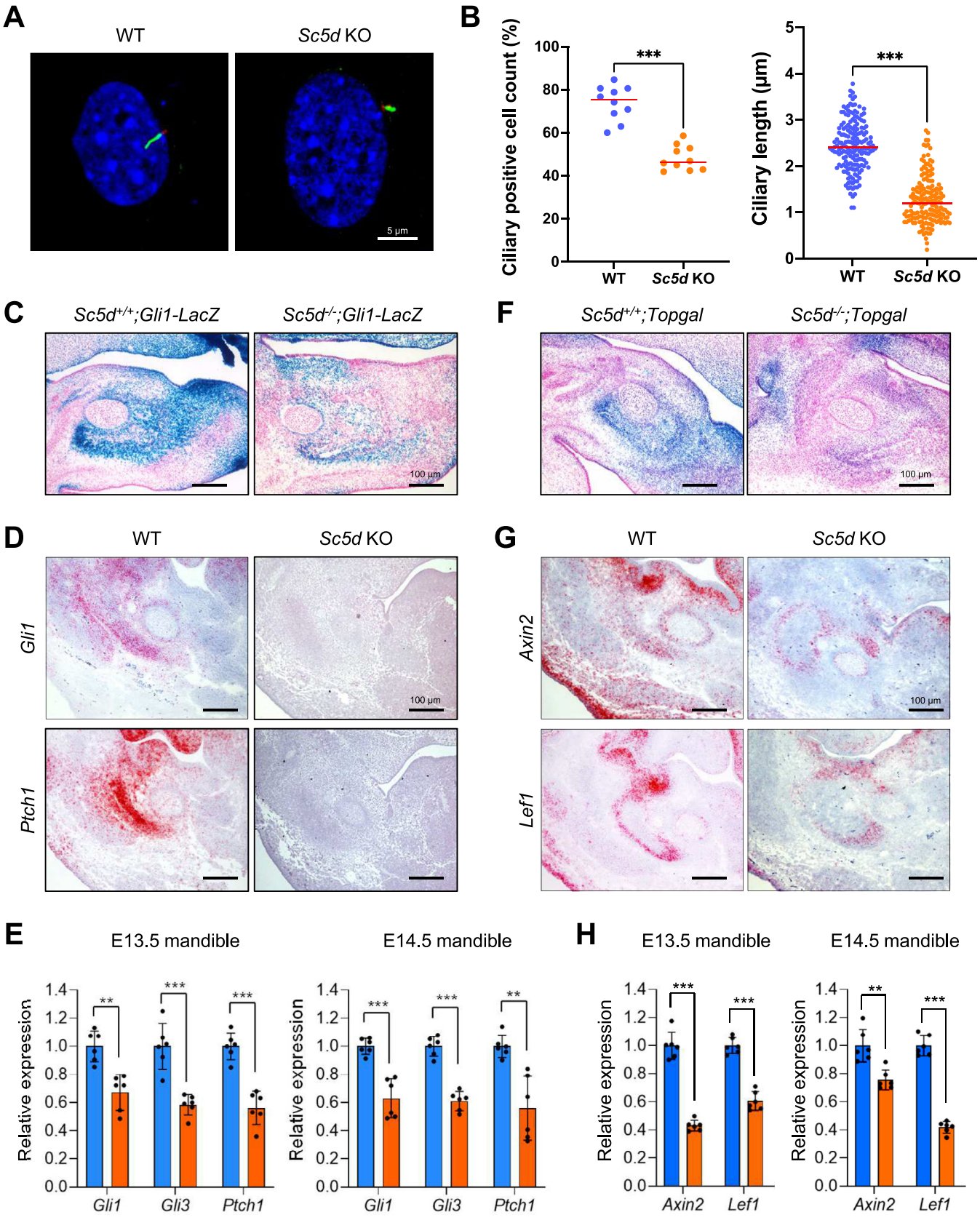
A
WT
Sc5d KO
5 μm
B
Ciliary positive cell count (%)
***
WT
Sc5d KO
Ciliary length (μm)
***
WT
Sc5d KO
C
Sc5d+/+;Gli1-LacZ
Sc5d-/-;Gli1-LacZ
100 μm
F
Sc5d+/+;Topgal
Sc5d-/-;Topgal
100 μm
D
WT
Sc5d KO
Gli1
Ptch1
100 μm
G
WT
Sc5d KO
Axin2
Lef1
100 μm
E
E13.5 mandible
E14.5 mandible
Relative expression
Gli1
Gli3
Ptch1
H
E13.5 mandible
E14.5 mandible
Relative expression
Axin2
Lef1

in the mandible of *Sc5d* KO mice, compared to that of WT control mice, at E12.5, E13.5, and E14.5 (Fig. 2C). Taken together, we conclude that the defects in osteogenesis in *Sc5d* KO mice were not caused by defects in osteoblast survival and proliferation.

Defects in osteoblast differentiation in Sc5d KO mice

Next, to identify the cellular mechanism underlying the dysregulated bone formation in *Sc5d* KO mice, we investigated osteoblast differentiation and extracellular matrix deposition in the developing mandible of *Sc5d* KO and WT control mice. We found that deposition of bone matrix, type I collagen (COL1), and secreted phosphoprotein 1 (SPP1; a.k.a. Osteopontin) from mature osteoblasts was apparently decreased in *Sc5d* KO mice compared to WT control mice (Fig. 2D, E), indicating that osteoblast differentiation and extracellular matrix were compromised in the mutant mice. We confirmed that expression of *Col1a1* and *Spp1* was significantly decreased in the mandible of *Sc5d* KO mice compared to that of WT control mice at E13.5 and E14.5, at both the mRNA and protein expression levels (Fig. 2D, F). We further confirmed that *Sc5d* KO osteoblasts showed defects in osteogenic differentiation in cultured primary osteoblasts (Fig. S3B, C). Expression of RUNX2, a marker of initiation of osteoblast differentiation, was not altered in the mandible of *Sc5d* KO mice at E12.5, E13.5, and E14.5 (Fig. 2E, F; Fig. S2C, D).

Compromised primary cilia-mediated hedgehog and WNT/β-catenin signaling in Sc5d null osteoblasts

Our recent study shows that cholesterol metabolism plays a crucial role in the formation of primary cilia [8]. To investigate whether and how ciliogenesis was altered in *Sc5d* KO osteoblasts, we conducted immunocytochemical analyses for the primary cilia and found that their length in *Sc5d* KO osteoblasts was shorter than in WT control osteoblasts, and that the number of ciliated *Sc5d* KO osteoblasts was lower than that seen in WT control osteoblasts in cell culture and in the mandibles of E13.5 and E14.5 embryos (Fig. 3A, B; Fig. S4A–C). The primary cilia can regulate HH and WNT/β-catenin signaling [12–14]; therefore, we hypothesized that HH and WNT/β-catenin signaling was compromised due to a failure in primary cilium formation in *Sc5d* KO osteoblasts. First, to evaluate HH signaling activity, we employed *Gli1-LacZ* reporter mice and found that HH signaling activity was suppressed in osteoblasts in *Sc5d*$^{-/-}$*;Gli1-LacZ* KO mice compared to *Sc5d*$^{+/+}$*;Gli1-LacZ* WT control mice at E13.5 (Fig. 3C). Furthermore, we performed *in situ* hybridization and quantitative RT-PCR for genes regulated by HH signaling (*Gli1*, *Gli3*, and *Ptch1*) and found that HH signaling was downregulated in the developing mandible of *Sc5d* KO mice (Fig. 3D, E).

Next, we analyzed WNT/β-catenin signaling activity with *Topgal* reporter mice and found that signaling was suppressed in osteoblasts in *Sc5d*$^{-/-}$*;Topgal* mice, compared to *Sc5d*$^{+/+}$*;Topgal* control mice, at E13.5 (Fig. 3F). Furthermore, we confirmed that WNT/β-catenin signaling was downregulated in the developing mandible of *Sc5d* KO mice with *in situ* hybridization and quantitative RT-PCR for genes regulated by WNT/β-catenin signaling (*Axin2* and *Lef1*) (Fig. 3G, *H*).

To confirm that expression of *Col1a1* and *Spp1* was directly regulated through WNT/β-catenin and HH signaling, we treated osteoblasts isolated from *Sc5d* KO and WT control mice with Lithium Chloride (LiCl) or WNT3A for inducing WNT/β-catenin signaling, and with Smoothened agonist (SAG) for inducing HH signaling, and found that expression of *Col1a1* and *Spp1* was induced in WT control osteoblasts, but not in *Sc5d* KO osteoblasts (Fig. 4A–*C*). In addition, we confirmed that the activation of either HH and WNT/β-catenin signaling pathway partially induced osteogenic differentiation in *Sc5d* KO osteoblasts (Fig. 4D). Our previous study showed that the *Col1a1* promoter contains the GLI-binding motif (5′-CACCACCCA-3′: −68 bp to −60 bp) and LEF1-binding motifs (minimal core sites: 5′-CTTTG-3′; −29 bp to −25 bp) [8]. We confirmed that both HH and WNT/β-catenin signaling pathways could directly regulate *Col1a1* expression (Fig. 4E, F). Similarly, we analyzed the promoter region of *Spp1* and found that there were three GLI-binding motifs and three LEF1-binding motifs (Fig. S5). LEF1, but not GLI, bound to the *Spp1* promoter region in chromatin immunoprecipitation (ChIP) assays (Fig. 4G, *H*), indicating that *Spp1* expression is regulated through WNT/β-catenin signaling. Taken together, our results show that HH and WNT/β-catenin signaling can differentially regulate expression of COL1 and SPP1, leading to intramembranous ossification defects.

To further confirm the functional significance of proper cholesterol metabolism in the regulation of primary cilium-related HH and WNT/β-catenin signaling in osteoblast differentiation, we conducted rescue experiments with simvastatin, a drug that can normalize cholesterol metabolism. We found that gene and protein expression of *Col1a1* and *Spp1* was almost completely restored in osteoblasts treated with simvastatin (Fig. 5A, B). Furthermore, we confirmed that defects in osteogenic differentiation in *Sc5d* KO osteoblasts were partially rescued with simvastatin through primary cilia-mediated HH and WNT/β-catenin signaling pathways (Fig. 5C–F).

Discussion

Various molecules are modified with cholesterol, but the role of cholesterol modification remains largely unknown [15–19]. The accumulation of immature cholesterol intermediates caused by mutations in genes crucial for cholesterol synthesis may have a different compensational capability in function. Lathosterolosis is a

Fig. 3. Failure in ciliogenesis leading to the suppression of hedgehog signaling in *Sc5d* null osteoblasts. (*A*) Immunocytochemical analysis for acetylated tubulin (primary cilium: green) and γ-tubulin (basal body: red) in cultured osteoblasts isolated from E18.5 *Sc5d* null (right) and WT control (left) mice. DAPI was used for counterstaining (blue). Scale bar, 5 μm. (*B*) Quantification of the number of ciliated cells (left) and the length of the primary cilia (right) in cultured osteoblasts isolated from E18.5 *Sc5d* null and WT control mice using 6 randomly selected fields from *A*. ***$p < 0.001$. (*C*) β-galactosidase staining (blue) at the intramembranous ossification region of the mandible in *Sc5d*$^{-/-}$*;Gli1-LacZ* (right, mutant) and *Sc5d*$^{+/+}$*;Gli1-LacZ* (left, control) mice at E14.5. Nuclear Fast Red was used for counterstaining (red). MC, Meckel's cartilage. Scale bars, 50 μm. (*D*) *In situ* hybridization for *Gli1* and *Ptch1* in coronal sections of the mandible of E14.5 wt (left) and *Sc5d* KO (right) mice. Hematoxylin was used for counterstaining (blue). Scale bars, 100 μm. (*E*) Relative mRNA expression for readout genes for the hedgehog signaling in the mandible of *Sc5d* null (orange bars) and WT control (blue bars) mice at E13.5 (left) and E14.5 (right). ***$p < 0.001$; *$p < 0.05$. (*F*) β-galactosidase staining (blue) at the intramembranous ossification region of the mandible in *Sc5d*$^{-/-}$*;Topgal* (right, mutant) and *Sc5d*$^{+/+}$*;Topgal* (left, control) mice at E14.5. Nuclear Fast Red was used for counterstaining (red). MC, Meckel's cartilage. Scale bars, 50 μm. (*G*) *In situ* hybridization for *Axin2* and *Lef1* in coronal sections of the mandible from E14.5 wild-type (WT, left) and *Sc5d* KO (right) mice. Hematoxylin was used for counterstaining (red). Scale bars, 100 μm. (*H*) Relative mRNA expression for readout genes for the WNT/β-catenin signaling in the mandible of *Sc5d* null (orange bars) and WT control (blue bars) mice at E13.5 (left) and E14.5 (right). ***$p < 0.001$; *$p < 0.05$. (For interpretation of the references to color in this figure legend, the reader is referred to the web version of this article.)

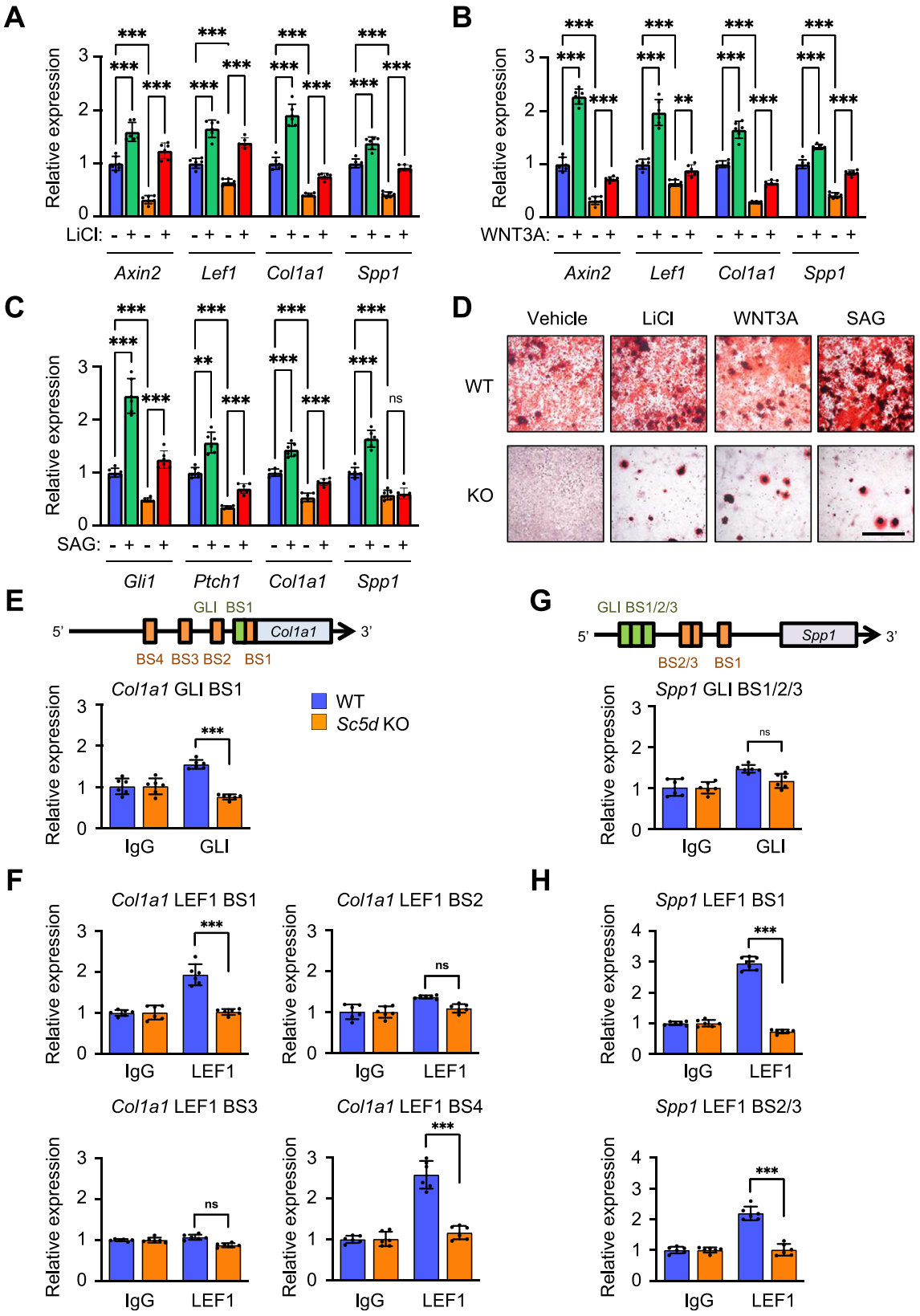
A
Relative expression
LiCl:
Axin2
Lef1
Col1a1
Spp1
B
Relative expression
WNT3A:
Axin2
Lef1
Col1a1
Spp1
C
Relative expression
SAG:
Gli1
Ptch1
Col1a1
Spp1
ns
D
Vehicle
LiCl
WNT3A
SAG
WT
KO
E
GLI BS1
5'
Col1a1
3'
BS4 BS3 BS2 BS1
Col1a1 GLI BS1
WT
Sc5d KO
Relative expression
IgG
GLI
G
GLI BS1/2/3
5'
Spp1
3'
BS2/3 BS1
Spp1 GLI BS1/2/3
Relative expression
ns
IgG
GLI
F
Col1a1 LEF1 BS1
Col1a1 LEF1 BS2
Col1a1 LEF1 BS3
Col1a1 LEF1 BS4
Relative expression
IgG
LEF1
ns
H
Spp1 LEF1 BS1
Spp1 LEF1 BS2/3
Relative expression
IgG
LEF1

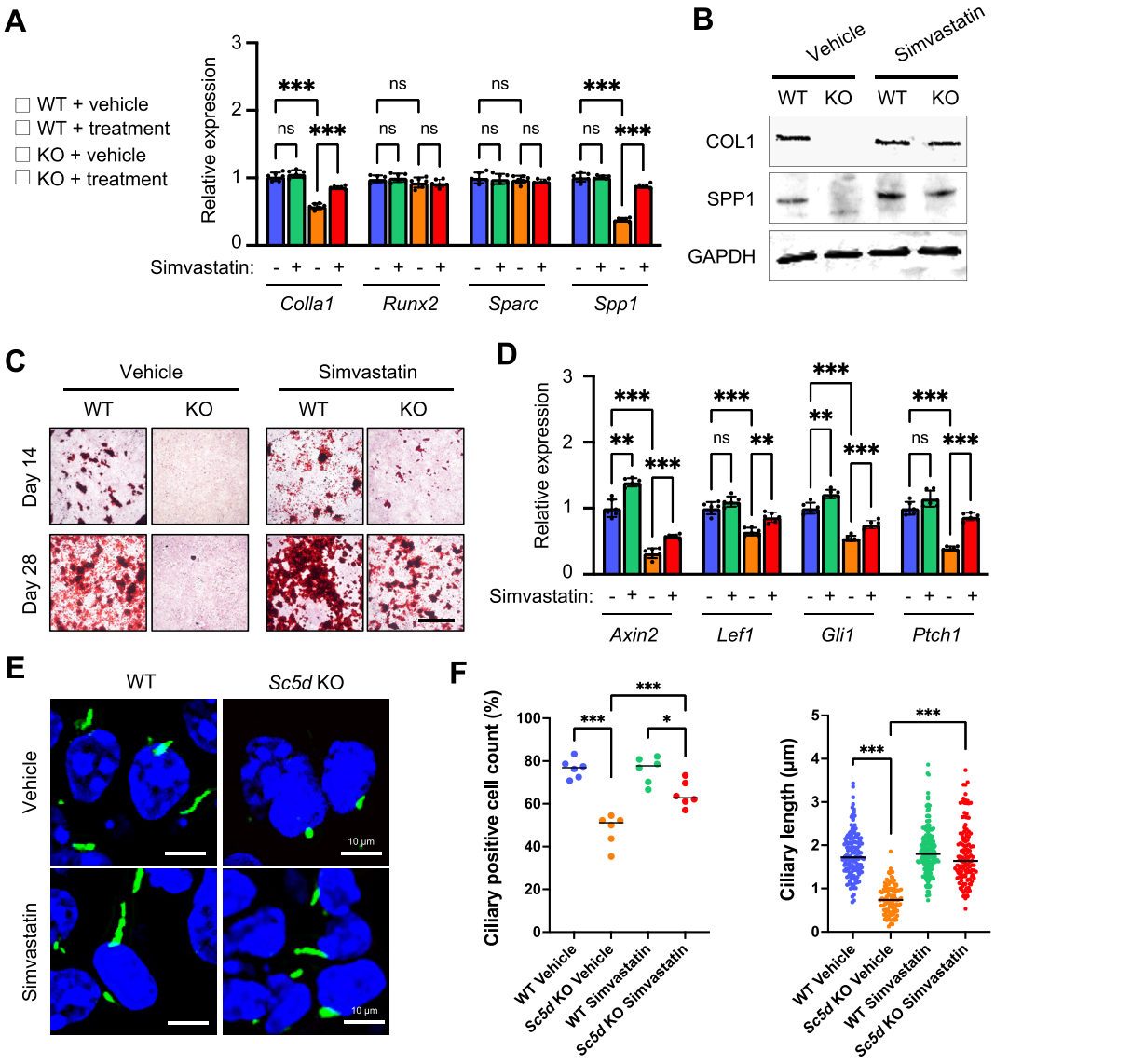

Fig. 5. Normalized osteogenic differentiation in *Sc5d* osteoblasts with simvastatin treatment. (*A*) Quantitative RT-PCR for the indicated genes in cultured *Sc5d* null (orange and red bars) and WT control (blue and green bars) osteoblasts treated with simvastatin or vehicle. ns, not significant; $^{**}p < 0.01$; $^{***}p < 0.001$. (*B*) Immunoblotting of COL1, SPP1, and GAPDH (an internal control) in cultured primary osteoblasts treated with simvastatin or vehicle. (*C*) Alizarin Red staining at 14 and 28 days of osteogenic differentiation in cultured primary osteoblasts treated with simvastatin or vehicle. (*D*) Quantitative RT-PCR for *Axin2* and *Lef1* for WNT/β-catenin signaling and *Gli1* and *Ptch1* for HH signaling in cultured *Sc5d* null (orange and red bars) and WT control (blue and green bars) osteoblasts treated with simvastatin or vehicle. (*E*) Immunocytochemical analysis for acetylated tubulin (primary cilium, green) and γ-tubulin (basal body, red) in cultured *Sc5d* KO (right) and WT control (left) osteoblasts treated with simvastatin or vehicle. DAPI was used for counterstaining (blue). Scale bar, 5 μm. (*F*) Quantification of the number of ciliated cells (left) and length of the primary cilia (right) in cultured *Sc5d* KO (orange) and WT control osteoblasts. $^{***}p < 0.001$. (For interpretation of the references to color in this figure legend, the reader is referred to the web version of this article.)

Fig. 4. Regulation of expression of *Col1a1* and *Spp1* by HH and WNT/β-catenin signaling. (*A*) Quantitative RT-PCR for the indicated genes in cultured *Sc5d* null (orange and red bars) and WT control (blue and green bars) osteoblasts treated with LiCl or vehicle. $^{***}p < 0.001$. (*B*) Quantitative RT-PCR for the indicated genes in cultured *Sc5d* null (orange and red bars) and WT control (blue and green bars) osteoblasts treated with WNT3A or vehicle. $^{**}p < 0.01$; $^{***}p < 0.001$. (*C*) Quantitative RT-PCR for the indicated genes in cultured *Sc5d* null (orange and red bars) and WT control (blue and green bars) osteoblasts treated with SAG or vehicle. $^{**}p < 0.01$; $^{***}p < 0.001$. (*D*) Alizarin Red staining at 14 days of osteogenic differentiation in cultured primary osteoblasts treated with vehicle, LiCl, WNT3A, or SAG. (*E*) Schematic diagram (top) of binding sites (BSs) for LEF1/active β-catenin (green) and GLI (orange) in the promoter region (5 kb upstream from transcription start site) of *Col1a1*. Conserved BSs among 3 species were selected for experimental validation. Chromatin immunoprecipitation (ChIP) assay using anti-GLI antibody on *Col1a1* in cultured osteoblasts from *Sc5d* null (orange bars) and WT control (blue bars) mice. ns, not significant; $^{***}p < 0.001$. (*F*) ChIP assay using anti-LEF1 antibody on *Col1a1* in cultured osteoblasts from *Sc5d* null (orange bars) and WT control (blue bars) mice. ns, not significant; $^{***}p < 0.001$. (*G*) Schematic diagram (top) of binding sites (BSs) for LEF1/active β-catenin (green) and GLI (orange) in the promoter region (5 kb upstream from transcription start site) of *Spp1*. Conserved BSs among 3 species were selected for experimental validation. ChIP assay using anti-GLI antibody on *Spp1* in cultured osteoblasts from *Sc5d* null (orange bars) and WT control (blue bars) mice. ns, not significant. (*H*) ChIP assay using anti-LEF1 antibody on *Spp1* in cultured osteoblasts from *Sc5d* null (orange bars) and WT control (blue bars) mice. $^{***}p < 0.001$. (For interpretation of the references to color in this figure legend, the reader is referred to the web version of this article.)

very rare autosomal recessive congenital disorder caused by mutations in *SC5D* [1,20]. To date, since only six patients have been reported, mutations in *SC5D* would lead to defects in early embryogenesis and miscarriages. Patients with lathosterolosis present a variety of clinical symptoms, including global developmental delay, cataracts, microcephaly and brain defects, as well as polydactyly and syndactyly, and craniofacial dysmorphology including micrognathia and a high arched palate [21–23]. In this study, we found that both HH and WNT/β-catenin signaling pathways are compromised in *Sc5d* KO mice. Our results show that the number of ciliated cells, as well as cilium length, is decreased in *Sc5d* KO osteoblasts, which is responsible for decreased HH and WNT/β-catenin signaling.

In the absence of HH ligands, Patched 1 (PTCH1) inhibits the translocation of Smoothened (SMO1) from the ciliary poach to the ciliary membrane. On the other hand, in the presence of HH ligands, PTCH1 undergoes endocytosis and ubiquitination, which induces translocation of SMO1 onto the primary cilia [24,25]. Importantly, the interaction of cholesterol located on the ciliary membrane with SMO1 is crucial for transduction of HH signaling via inactivation of PTCH1 [26–30]. A recent study shows that cholesterol in the plasma membrane acts as a second messenger between PTCH1 and SMO1 [30].

Interestingly, DHCR7, which is a cholesterol biosynthesis enzyme, localizes near the base of the primary cilium and activates HH signaling, whereas stimulation of the HH signaling suppresses activity of DHCR7 and removes it from the primary cilium [31]. HH stimulation activates the cholesterol 7 alpha-hydroxylase (CYP7A1), which accumulates near the ciliary base and produces oxysterols that promote HH signaling [31]. Therefore, HH signaling might be affected through both deficient ciliogenesis and abnormal composition of the ciliary membrane. However, cholesterol amounts, as well as localization of cholesterol synthesis enzymes around the ciliary membrane, may directly affect the functions of primary cilia. Pharmacological cholesterol depletion in zebrafish embryos results in shorter and less frequent primary cilia, leading to ciliopathy-like phenotypes, such as left–right asymmetry and heart developmental defects [32]. In addition, depletion of TMEM135 (transmembrane protein 135) in Huh7 cells, a human hepatoma-derived cell line, causes lysosomal cholesterol accumulation, which results in shorter primary cilia by impaired trafficking of Rab8 to the centrioles [33]. Patients with Zellweger syndrome (ZS), an autosomal recessive peroxisome-deficient disorder, exhibit ciliopathy-like features. Fibroblasts from ZS patients and *PEX1/14* double knockout cells contain less cholesterol in the ciliary membrane, resulting in downregulated HH signaling via delocalization of SMO1 on the primary cilium, although the length and number of the primary cilium remain intact [34]. These results suggest that not only cholesterol amounts in primary cilia but also intracellular cholesterol distribution plays a crucial role in ciliogenesis and HH signaling.

In contrast to HH signaling, the role of cholesterol metabolism in WNT signaling remains largely unknown. A previous study showed that binding of cholesterol-bound Dishevelled 2 (Dvl2) to Frizzled 7 (Fzd7) and subsequent activation of canonical Wnt/β-catenin signaling is greater than that of non-cholesterol-bound Dvl2 in *Xenopus* embryos [35]. Binding of cholesterol to Fzd5, a Wnt receptor, at the extracellular linker region enhances palmitoylation, which is crucial for maturation and trafficking of Fzd5 to the plasma membrane [36]. Exogenous cholesterol supplementation in Wnt-addicted pancreatic ductal adenocarcinoma cells enhances canonical WNT/β-catenin signaling via Fzd5, resulting in tumor growth [36]. Zebrafish with homozygous mutations in the 3-hydroxy-3-methylglutaryl-CoA synthase 1 gene (*Hmgcs1*) at the Vu57 allele, which encodes the first enzyme in the cholesterol synthesis pathway, exhibit severe craniofacial anomalies, including complete absence of Meckel's, ceratohyal, and ceratobranchial cartilages due to suppression of Wnt/β-catenin signaling [37,38]. Interestingly, activation of Wnt signaling can restore the craniofacial defects in *Hmgcs1* mutant zebrafish [37,38]. These results suggest that activation of WNT signaling is at least partially dependent on cholesterol metabolism.

Our previous study showed that mice with a deficiency in *Dhcr7*, another enzyme crucial for cholesterol synthesis that acts right after the SC5D enzymatic reaction, exhibit accelerated calvarial bone formation due to upregulated WNT/β-catenin signaling [8]. Interestingly, WNT/β-catenin signaling was altered in a different manner between *Sc5d* KO and *Dhcr7* KO osteoblasts, while HH signaling was suppressed in both *Sc5d* KO and *Dhcr7* KO osteoblasts due to defective ciliogenesis. There are several possibilities for the underlying cell and tissue-specific regulatory mechanisms: 1) difference in the toxicity of each cholesterol intermediate, and 2) difference in molecules (accessory proteins etc.) and complexes involved in the pathway. In this study, we found that there was no change in cell proliferation and survival so that accumulation of cholesterol intermediates might not be toxic together with the effects on HH and WNT/β-catenin signaling. Previous studies suggest that acylation, esterification, and conjugation of cholesterol and phospholipid on WNT3A, a canonical WNT ligand, play a crucial role in its stabilization and activation [39–41]. A recent study shows that 7-dehydrocholesterol (7-DHC) can partially compensate for the functions of mature cholesterol in Clathrin-mediated endocytosis [42]. Interestingly, stabilization of endocytic vesicles is affected by cholesterol's synthetic status; vesicles containing 7-DHC are the most stable, followed by mature cholesterol, desmosterol, and lanosterol [43]. Therefore, aberrations in cholesterol synthesis may affect signaling activity through endocytosis.

Regarding the bone phenotype, previous studies show that HH signaling plays crucial roles in limb and digit development [44–46]. For example, *Gli3* conditional KO (*Shh-Cre;Gli3*$^{Xt\text{-}J/Xt\text{-}J}$ and *Prx1-Cre;Gli3*$^{Xt\text{-}J/Xt\text{-}J}$) as well as *Gli3* null mice exhibit preaxial polydactyly [47,48]. A hypomorphic mutation or spontaneous deletion of *Ptch1* in *Ptch1*$^{dl/dl}$ and *Ptch1*$^{mes/mes}$ mice, respectively, results in preaxial polydactyly [49,50]. *Shh* null mice lack all digits, tibiae, and fibulae [51], whereas mice with ectopic expression of *Shh* in epithelial cell lineages (*K14-Shh*) exhibit polysyndactyly, absence of calvarial bones, a hypoplastic mandible, and cleft palate due to expansion and increase of SHH signaling [52], suggesting that gradient SHH signaling plays a crucial role in the determination of digit number and identification. Moreover, mice without cholesterol modification on SHH (*Sox2-Cre;Shh*$^{N/+}$) exhibit preaxial polydactyly due to widespread SHH signaling, suggesting that proper cholesterol modification on SHH is essential for the determination of digit number and identity [53]. Mice with mutations in *Ihh*, an endochondral ossification morphogen (*Ihh*$^{E95K/E95K}$ mice), exhibit brachydactyly, but not polydactyly [54]. Similar to mice with loss of HH signaling, mice with dysregulated WNT signaling display limb and digit phenotypes. For example, *Dkk1* null mice exhibit polydactyly or syndactyly [55]; *Lrp4* deficient mice exhibit oligodactyly or syndactyly [56]. The limb and digit phenotypes in *Sc5d* KO mice are different in severity and location from those in mice with loss of either HH or WNT signaling. Taken together, the phenotypic features in *Sc5d* KO mice are likely caused by a combination of dysregulated WNT and SHH signaling pathways due to defects in ciliogenesis. Indeed, loss of ciliary proteins results in defects in limb and digit development, as seen in *Sc5d* KO mice. For instance, mice deficient for ciliary proteins (e.g. *Prx1-Cre;Ift88*$^{F/-}$ [57], *Prx1-Cre;Kif3*$^{F/-}$ [57], and *Ift80* null mice [58]) display

preaxial polydactyly, dysregulated endochondral ossification, and shorter long bones. *Tbx3* null mice exhibit agenesis of the ulna, fibula, and most of digits [59], and *Prx1-Cre;Tbx3* conditional KO mice exhibit preaxial polydactyly and postaxial oligodactyly in the forelimbs [59].

There are some differences in endochondral and intramembranous ossification in *Sc5d* KO mice. Endochondral ossification forms the majority of trunk bones, whereas intramembranous ossification forms the majority of craniofacial bones. In the limbs and digits, cartilage formation is dysregulated, resulting in bent shorter bones, as well as polysyndactyly, in the middle phalanges or syndactyly. Interestingly, there is no obvious bone defect in the trunk, limbs, and digits in mice deficient for *Dhcr7*, which have loss of mature cholesterol as well as accumulation of cholesterol intermediates, 7-dehydrodesmosterol and 7-dehydrocholesterol. Taken together, the digit malformation and endochondral ossification defect in *Sc5d* KO mice are likely caused by abnormally accumulated cholesterol intermediates, lathosterol and dehydrolathosterol, but not by lack of mature cholesterol.

Conclusion

In this study, we demonstrated the role of cholesterol metabolism in the regulation of osteogenesis and ciliogenesis using *Sc5d* KO mice. *Sc5d* KO osteoblasts displayed fewer and shorter primary cilia compared to controls. The disruption of ciliogenesis led to the suppression of HH and WNT/β-catenin signaling, resulting in downregulation of the expression of *Col1a1* and *Spp1*. The principles learned from this study may lead to the development of innovative therapeutic approaches for bone diseases related to cholesterol metabolic aberrations.

Compliance with ethics requirements.

This article does not include any studies with human subjects. All animal experiments were reviewed and approved by the Animal Welfare Committee (AWC) and the Institutional Animal Care and Use Committee of UTHealth (AWC 22–0087). All methods were performed in accordance with the relevant guidelines and regulations provided by ARRIVE (Animal Research: Reporting of *In Vivo* Experiments).

CRediT authorship contribution statement

Chihiro Iwaya: Investigation, Methodology, Visualization, Writing – review & editing. **Akiko Suzuki:** Conceptualization, Investigation, Methodology, Visualization, Writing – original draft, Writing – review & editing. **Junichi Iwata:** Funding acquisition, Supervision, Conceptualization, Investigation, Methodology, Writing – original draft, Writing – review & editing.

Declaration of competing interest

The authors declare that they have no known competing financial interests or personal relationships that could have appeared to influence the work reported in this paper.

Acknowledgements

We thank the MicroCT Lab of Baylor College of Medicine for technical assistance. We thank Dr. Forbes D. Porter at The Eunice Kennedy Shriver National Institute of Child Health and Human Development (NICHD), National Institutes of Health (NIH), for providing the *Sc5d* KO mice, and technical assistance from Yurie Mikami, Junbo Shim, and Hiroki Yoshioka. This study was supported by grants from the National Institute of Dental and Craniofacial Research (NIDCR), NIH (R01DE026767 and R01DE029818 to JI), and UTHealth School of Dentistry faculty funding to JI.

Appendix A. Supplementary data

Supplementary data to this article can be found online at https://doi.org/10.1016/j.jare.2023.12.008.

References

[1] Porter FD, Herman GE. Malformation syndromes caused by disorders of cholesterol synthesis. J Lipid Res 2011;52(1):6–34. doi: https://doi.org/10.1194/jlr.R009548. PubMed PMID: 20929975; PubMed Central PMCID: PMC2999931.
[2] Suzuki A, Minamide M, Iwaya C, Ogata K, Iwata J. Role of metabolism in bone development and homeostasis. International journal of molecular sciences 2020;21(23). doi: https://doi.org/10.3390/ijms2123899. Epub 20201126. PubMed PMID: 33256181; PubMed Central PMCID: PMCPMC7729585.
[3] Krakowiak PA, Wassif CA, Kratz L, Cozma D, Kovarova M, Harris G, et al. Lathosterolosis: An inborn error of human and murine cholesterol synthesis due to lathosterol 5-desaturase deficiency. Hum Mol Genet 2003;12(13):1631–41. PubMed PMID: 12812989.
[4] Lin X, Patil S, Gao YG, Qian A. The bone extracellular matrix in bone formation and regeneration. Front Pharmacol 2020;11:757. doi: https://doi.org/10.3389/fphar.2020.00757. PubMed PMID: 32528290; PubMed Central PMCID: PMC7264100.
[5] Emmer BT, Maric D, Engman DM. Molecular mechanisms of protein and lipid targeting to ciliary membranes. J Cell Sci 2010;123(Pt 4):529–36. doi: https://doi.org/10.1242/jcs.062968. PubMed PMID: 20145001; PubMed Central PMCID: PMC2818192.
[6] Chang CF, Schock EN, Attia AC, Stottmann RW, Brugmann SA. The ciliary baton: Orchestrating neural crest cell development. Curr Top Dev Biol 2015;111:97–134. doi: https://doi.org/10.1016/bs.ctdb.2014.11.004. PubMed PMID: 25662259.
[7] Nachury MV, Seeley ES, Jin H. Trafficking to the ciliary membrane: How to get across the periciliary diffusion barrier? Annu Rev Cell Dev Biol 2010;26:59–87. doi: https://doi.org/10.1146/annurev.cellbio.042308.113337. PubMed PMID: 19575670; PubMed Central PMCID: PMC2952038.
[8] Suzuki A, Ogata K, Yoshioka H, Shim J, Wassif CA, Porter FD, et al. Disruption of Dhcr7 and Insig1/2 in cholesterol metabolism causes defects in bone formation and homeostasis through primary cilium formation. Bone Res 2020;8:1. doi: https://doi.org/10.1038/s41413-019-0078-3. PubMed PMID: 31934493; PubMed Central PMCID: PMC6946666.
[9] Suzuki A, Pelikan RC, Iwata J. WNT/beta-catenin signaling regulates multiple steps of myogenesis by regulating step-specific targets. Mol Cell Biol 2015;35(10):1763–76. doi: https://doi.org/10.1128/MCB.01180-14. PubMed PMID: 25755281; PubMed Central PMCID: PMC4405648.
[10] Kinzler KW, Vogelstein B. The GLI gene encodes a nuclear protein which binds specific sequences in the human genome. Mol Cell Biol 1990;10(2):634–42. PubMed PMID: 2105456; PubMed Central PMCID: PMC360861.
[11] Winklmayr M, Schmid C, Laner-Plamberger S, Kaser A, Aberger F, Eichberger T, et al. Non-consensus GLI binding sites in Hedgehog target gene regulation. BMC Mol Biol 2010;11:2. doi: https://doi.org/10.1186/1471-2199-11-2. PubMed PMID: 20070907; PubMed Central PMCID: PMC2830928.
[12] Kopinke D, Norris AM, Mukhopadhyay S. Developmental and regenerative paradigms of cilia regulated hedgehog signaling. Semin Cell Dev Biol 2021;110:89–103. doi: https://doi.org/10.1016/j.semcdb.2020.05.029. PubMed PMID: 32540122; PubMed Central PMCID: PMC7736055.
[13] Anvarian Z, Mykytyn K, Mukhopadhyay S, Pedersen LB, Christensen ST. Cellular signalling by primary cilia in development, organ function and disease. Nat Rev Nephrol 2019;15(4):199–219. doi: https://doi.org/10.1038/s41581-019-0116-9. PubMed PMID: 30733609; PubMed Central PMCID: PMC6426138.
[14] Wheway G, Nazlamova L, Hancock JT. Signaling through the primary cilium. Front Cell Dev Biol 2018;6:8. doi: https://doi.org/10.3389/fcell.2018.00008. PubMed PMID: 29473038; PubMed Central PMCID: PMC5809511.
[15] Jeong J, McMahon AP. Cholesterol modification of Hedgehog family proteins. J Clin Invest 2002;110(5):591–6. doi: https://doi.org/10.1172/JCI16506. PubMed PMID: 12208857; PubMed Central PMCID: PMC151115.
[16] Purohit R, Peng DS, Vielmas E, Ondrus AE. Dual roles of the sterol recognition region in Hedgehog protein modification. Communications biology 2020;3(1):250. doi: https://doi.org/10.1038/s42003-020-0977-2. PubMed PMID: 32440000; PubMed Central PMCID: PMC7242414.
[17] Sheng R, Chen Y, Yung Gee H, Stec E, Melowic HR, Blatner NR, et al. Cholesterol modulates cell signaling and protein networking by specifically interacting with PDZ domain-containing scaffold proteins. Nat Commun 2012;3:1249. doi: https://doi.org/10.1038/ncomms2221. PubMed PMID: 23212378; PubMed Central PMCID: PMC3526836.
[18] Dubey V, Bozorg B, Wustner D, Khandelia H. Cholesterol binding to the sterol-sensing region of Niemann Pick C1 protein confines dynamics of its N-terminal domain. PLoS Comput Biol 2020;16(10):e1007554. doi: https://doi.org/10.1371/journal.pcbi.1007554. PubMed PMID: 33021976; PubMed Central PMCID: PMC7537887.

[19] Fantini J, Barrantes FJ. How cholesterol interacts with membrane proteins: An exploration of cholesterol-binding sites including CRAC, CARC, and tilted domains. Front Physiol 2013;4:31. doi: https://doi.org/10.3389/fphys.2013.00031. PubMed PMID: 23450735; PubMed Central PMCID: PMC3584320.
[20] Brunetti-Pierri N, Corso G, Rossi M, Ferrari P, Balli F, Rivasi F, et al. Lathosterolosis, a novel multiple-malformation/mental retardation syndrome due to deficiency of 3beta-hydroxysteroid-delta5-desaturase. Am J Hum Genet 2002;71(4):952–8. doi: https://doi.org/10.1086/342668. PubMed PMID: 12189593; PubMed Central PMCID: PMC378549.
[21] Platt FM, Wassif C, Colaco A, Dardis A, Lloyd-Evans E, Bembi B, et al. Disorders of cholesterol metabolism and their unanticipated convergent mechanisms of disease. Annu Rev Genomics Hum Genet 2014;15:173–94. doi: https://doi.org/10.1146/annurev-genom-091212-153412. PubMed PMID: 25184529; PubMed Central PMCID: PMC6292211.
[22] Anderson R, Rust S, Ashworth J, Clayton-Smith J, Taylor RL, Clayton PT, et al. Lathosterolosis: A relatively mild case with cataracts and learning difficulties. JIMD reports 2019;44:79–84. doi: https://doi.org/10.1007/8904_2018_127. PubMed PMID: 30097991; PubMed Central PMCID: PMC6323057.
[23] Prasun P, Ferguson E, Iverson A, Cork E, Dolinger M, Ward SC, et al. Lathosterolosis: An extremely rare inherited condition associated with progressive liver disease. J Pediatr Gastroenterol Nutr 2019;69(5):e142–5. doi: https://doi.org/10.1097/MPG.0000000000002434. PubMed PMID: 31259789.
[24] May EA, Sroka TJ, Mick DU. Phosphorylation and ubiquitylation regulate protein trafficking, signaling, and the biogenesis of primary cilia. Front Cell Dev Biol 2021;9:664279. doi: https://doi.org/10.3389/fcell.2021.664279. PubMed PMID: 33912570; PubMed Central PMCID: PMC8075051.
[25] Nozawa YI, Lin C, Chuang PT. Hedgehog signaling from the primary cilium to the nucleus: an emerging picture of ciliary localization, trafficking and transduction. Curr Opin Genet Dev 2013;23(4):429–37. doi: https://doi.org/10.1016/j.gde.2013.04.008. PubMed PMID: 23725801; PubMed Central PMCID: PMC3913210.
[26] Kinnebrew M, Iverson EJ, Patel BB, Pusapati GV, Kong JH, Johnson KA, et al. Cholesterol accessibility at the ciliary membrane controls hedgehog signaling. Elife 2019;8. doi: https://doi.org/10.7554/eLife.50051. Epub 20191030 PubMed PMID: 31657721; PubMed Central PMCID: PMCPMC6850779.
[27] Weiss LE, Milenkovic L, Yoon J, Stearns T, Moerner WE. Motional dynamics of single Patched1 molecules in cilia are controlled by Hedgehog and cholesterol. Proc Natl Acad Sci U S A. 2019;116(12):5550–7. doi: https://doi.org/10.1073/pnas.1816747116. Epub 20190228 PubMed PMID: 30819883; PubMed Central PMCID: PMCPMC6431229.
[28] Raleigh DR, Sever N, Choksi PK, Sigg MA, Hines KM, Thompson BM, et al. Cilia-associated oxysterols activate smoothened. Mol Cell 2018;72(2):316–27 e5. doi: https://doi.org/10.1016/j.molcel.2018.08.034. PubMed PMID: 30340023; PubMed Central PMCID: PMCPMC6503851.
[29] Kinnebrew M, Woolley RE, Ansell TB, Byrne EFX, Frigui S, Luchetti G, et al. Patched 1 regulates Smoothened by controlling sterol binding to its extracellular cysteine-rich domain. Sci Adv 2022;8(22). doi: https://doi.org/10.1126/sciadv.abm5563. Epub 20220603. PubMed PMID: 35658032; PubMed Central PMCID: PMCPMC9166294.
[30] Radhakrishnan A, Rohatgi R, Siebold C. Cholesterol access in cellular membranes controls Hedgehog signaling. Nat Chem Biol 2020;16(12):1303–13. doi: https://doi.org/10.1038/s41589-020-00678-2. PubMed PMID: 33199907; PubMed Central PMCID: PMC7872078.
[31] Findakly S, Daggubati V, Garcia G, LaStella SA, Choudhury A, Tran C, et al. Sterol and oxysterol synthases near the ciliary base activate the Hedgehog pathway. J Cell Biol 2021;220(1). doi: https://doi.org/10.1083/jcb.202002026. PubMed PMID: 33284321; PubMed Central PMCID: PMCPMC7721912.
[32] Maerz LD, Burkhalter MD, Schilpp C, Wittekindt OH, Frick M, Philipp M. Pharmacological cholesterol depletion disturbs ciliogenesis and ciliary function in developing zebrafish. Communications biol 2019;2:31. doi: https://doi.org/10.1038/s42003-018-0272-7. Epub 20190129. PubMed PMID: 30729178; PubMed Central PMCID: PMCPMC6351647.
[33] Maharjan Y, Lee JN, Kwak SA, Dutta RK, Park C, Choe SK, et al. TMEM135 regulates primary ciliogenesis through modulation of intracellular cholesterol distribution. EMBO Rep 2020;21(5):e48901. doi: https://doi.org/10.15252/embr.201948901. Epub 20200311. PubMed PMID: 32157776; PubMed Central PMCID: PMCPMC7202201.
[34] Miyamoto T, Hosoba K, Itabashi T, Iwane AH, Akutsu SN, Ochiai H, et al. Insufficiency of ciliary cholesterol in hereditary Zellweger syndrome. EMBO J 2020;39(12):e103499. doi: https://doi.org/10.15252/embj.2019103499. PubMed PMID: 32368833; PubMed Central PMCID: PMC7298307.
[35] Sheng R, Kim H, Lee H, Xin Y, Chen Y, Tian W, et al. Cholesterol selectively activates canonical Wnt signalling over non-canonical Wnt signalling. Nat Commun 2014;5:4393. doi: https://doi.org/10.1038/ncomms5393. Epub 20140715 PubMed PMID: 25024088; PubMed Central PMCID: PMCPMC4100210.
[36] Zheng S, Lin J, Pang Z, Zhang H, Wang Y, Ma L, et al. Aberrant cholesterol metabolism and Wnt/beta-catenin signaling coalesce via Frizzled5 in supporting cancer growth. Adv Sci (Weinh) 2022;9(28):e2200750. doi: https://doi.org/10.1002/advs.202200750. Epub 20220817PubMed PMID: 35975457; PubMed Central PMCID: PMCPMC9534957.
[37] Quintana AM, Hernandez JA, Gonzalez CG. Functional analysis of the zebrafish ortholog of HMGCS1 reveals independent functions for cholesterol and isoprenoids in craniofacial development. PLoS One 2017;12(7):e0180856. doi: https://doi.org/10.1371/journal.pone.0180856. Epub 20170707 PubMed PMID: 28686747; PubMed Central PMCID: PMCPMC5501617.
[38] Castro VL, Reyes-Nava NG, Sanchez BB, Gonzalez CG, Paz D, Quintana AM. Activation of WNT signaling restores the facial deficits in a zebrafish with defects in cholesterol metabolism. Genesis 2020;58(12):e23397. doi: https://doi.org/10.1002/dvg.23397. Epub 20201116 PubMed PMID: 33197123; PubMed Central PMCID: PMCPMC7816230.
[39] Janda CY, Garcia KC. Wnt acylation and its functional implication in Wnt signalling regulation. Biochem Soc Trans 2015;43(2):211–6. doi: https://doi.org/10.1042/BST20140249. PubMed PMID: 25849919; PubMed Central PMCID: PMC4445369.
[40] Tuysuz N, van Bloois L, van den Brink S, Begthel H, Verstegen MM, Cruz LJ, et al. Lipid-mediated Wnt protein stabilization enables serum-free culture of human organ stem cells. Nat Commun 2017;8:14578. doi: https://doi.org/10.1038/ncomms14578. PubMed PMID: 28262686; PubMed Central PMCID: PMC5343445.
[41] Lee HJ, Li J, Vickman RE, Li J, Liu R, Durkes AC, et al. Cholesterol esterification inhibition suppresses prostate cancer metastasis by impairing the Wnt/beta-catenin pathway. Molecular cancer research : MCR 2018;16(6):974–85. doi: https://doi.org/10.1158/1541-7786.MCR-17-0665. PubMed PMID: 29545473; PubMed Central PMCID: PMC5984676.
[42] Anderson RH, Sochacki KA, Vuppula H, Scott BL, Bailey EM, Schultz MM, et al. Sterols lower energetic barriers of membrane bending and fission necessary for efficient clathrin-mediated endocytosis. Cell Rep 2021;37(7):110008. doi: https://doi.org/10.1016/j.celrep.2021.110008. PubMed PMID: 34788623; PubMed Central PMCID: PMC8620193.
[43] St Clair JW, London E. Effect of sterol structure on ordered membrane domain (raft) stability in symmetric and asymmetric vesicles. Biochim Biophys Acta 2019;1861(6):1112–22. doi: https://doi.org/10.1016/j.bbamem.2019.03.012. PubMed PMID: 30904407; PubMed Central PMCID: PMC6525066.
[44] Zhu J, Patel R, Trofka A, Harfe BD, Mackem S. Sonic hedgehog is not a limb morphogen but acts as a trigger to specify all digits in mice. Dev Cell 2022;57(17):2048–62 e4. doi: https://doi.org/10.1016/j.devcel.2022.07.016. Epub 20220816. PubMed PMID: 35977544; PubMed Central PMCID: PMCPMC9709693.
[45] Tickle C, Towers M. Sonic hedgehog signaling in limb development. Front Cell Dev Biol 2017;5(14). doi: https://doi.org/10.3389/fcell.2017.00014. Epub 20170228. PubMed PMID: 28293554; PubMed Central PMCID: PMCPMC5328949.
[46] Litingtung Y, Dahn RD, Li Y, Fallon JF, Chiang C. Shh and Gli3 are dispensable for limb skeleton formation but regulate digit number and identity. Nature 2002;418(6901):979–83. doi: https://doi.org/10.1038/nature01033. Epub 20020818. PubMed PMID: 12198547.
[47] Lopez-Rios J, Speziale D, Robay D, Scotti M, Osterwalder M, Nusspaumer G, et al. GLI3 constrains digit number by controlling both progenitor proliferation and BMP-dependent exit to chondrogenesis. Dev Cell 2012;22(4):837–48. doi: https://doi.org/10.1016/j.devcel.2012.01.006. Epub 20120329. PubMed PMID: 22465667; PubMed Central PMCID: PMCPMC4486391.
[48] Quinn ME, Haaning A, Ware SM. Preaxial polydactyly caused by Gli3 haploinsufficiency is rescued by Zic3 loss of function in mice. Hum Mol Genet 2012;21(8):1888–96. doi: https://doi.org/10.1093/hmg/dds002. Epub 20120110. PubMed PMID: 22234993; PubMed Central PMCID: PMCPMC3313802.
[49] Feng W, Choi I, Clouthier DE, Niswander L, Williams T. The Ptch1(DL) mouse: a new model to study lambdoid craniosynostosis and basal cell nevus syndrome-associated skeletal defects. Genesis 2013;51(10):677–89. doi: https://doi.org/10.1002/dvg.22416. Epub 20130830. PubMed PMID: 23897749; PubMed Central PMCID: PMCPMC3918964.
[50] Sweet HO, Bronson RT, Donahue LR, Davisson MT. Mesenchymal dysplasia: a recessive mutation on chromosome 13 of the mouse. J Hered 1996;87(2):87–95. doi: https://doi.org/10.1093/oxfordjournals.jhered.a022981. PubMed PMID: 8830098.
[51] Chiang C, Litingtung Y, Lee E, Young KE, Corden JL, Westphal H, et al. Cyclopia and defective axial patterning in mice lacking Sonic hedgehog gene function. Nature 1996;383(6599):407–13. doi: https://doi.org/10.1038/383407a0. PubMed PMID: 8837770.
[52] Cobourne MT, Xavier GM, Depew M, Hagan L, Sealby J, Webster Z, et al. Sonic hedgehog signalling inhibits palatogenesis and arrests tooth development in a mouse model of the nevoid basal cell carcinoma syndrome. Dev Biol 2009;331(1):38–49. doi: https://doi.org/10.1016/j.ydbio.2009.04.021. Epub 20090424. PubMed PMID: 19394325; PubMed Central PMCID: PMCPMC2696601.
[53] Li Y, Zhang H, Litingtung Y, Chiang C. Cholesterol modification restricts the spread of Shh gradient in the limb bud. Proc Natl Acad Sci U S A 2006;103(17):6548–53. doi: https://doi.org/10.1073/pnas.0600124103. PubMed PMID: 16611729; PubMed Central PMCID: PMC1458921.
[54] Gao B, Hu J, Stricker S, Cheung M, Ma G, Law KF, et al. A mutation in Ihh that causes digit abnormalities alters its signalling capacity and range. Nature 2009;458(7242):1196–200. doi: https://doi.org/10.1038/nature07862. Epub 20090301. PubMed PMID: 19252479.

[55] Mukhopadhyay M, Shtrom S, Rodriguez-Esteban C, Chen L, Tsukui T, Gomer L, et al. Dickkopf1 is required for embryonic head induction and limb morphogenesis in the mouse. Dev Cell 2001;1(3):423–34. doi: https://doi.org/10.1016/s1534-5807(01)00041-7. PubMed PMID: 11702953.
[56] Weatherbee SD, Anderson KV, Niswander LA. LDL-receptor-related protein 4 is crucial for formation of the neuromuscular junction. Development 2006;133 (24):4993–5000. doi: https://doi.org/10.1242/dev.02696. PubMed PMID: 17119023.
[57] Haycraft CJ, Zhang Q, Song B, Jackson WS, Detloff PJ, Serra R, et al. Intraflagellar transport is essential for endochondral bone formation. Development 2007;134(2):307–16. doi: https://doi.org/10.1242/dev.02732. Epub 20061213. PubMed PMID: 17166921.
[58] Rix S, Calmont A, Scambler PJ, Beales PL. An Ift80 mouse model of short rib polydactyly syndromes shows defects in hedgehog signalling without loss or malformation of cilia. Hum Mol Genet 2011;20(7):1306–14. doi: https://doi.org/10.1093/hmg/ddr013. Epub 20110112. PubMed PMID: 21227999; PubMed Central PMCID: PMCPMC3049354.
[59] Emechebe U, Kumar PP, Rozenberg JM, Moore B, Firment A, Mirshahi T, et al. T-box3 is a ciliary protein and regulates stability of the Gli3 transcription factor to control digit number. Elife 2016;5. doi: https://doi.org/10.7554/eLife.07897. Epub 20160405. PubMed PMID: 27046536; PubMed Central PMCID: PMCPMC4829432.